JOURNAL OF GEOPHYSICAL RESEARCH, VOL. 102, NO. C5, PAGES 10,499–10,507, MAY 15, 1997

A parametric model for the Yellow Sea thermal variability

Peter C. Chu and Charles R. Fralick Jr.
Naval Postgraduate School, Monterey, California

Steven D. Haeger and Michael J. Carron
Naval Oceanographic Office, Stennis Space Center, Mississippi

Abstract. A thermal parametric model has been developed for analyzing observed regional sea temperature profiles based on a layered structure of temperature fields (mixed layer, thermocline, and deep layers). It contains three major components: (1) a first-guess parametric model, (2) high-resolution profiles interpolated from observed profiles, and (3) fitting of high-resolution profiles to the parametric model. The output of this parametric model is a set of major characteristics of each profile: sea surface temperature, mixed-layer depth, thermocline depth, thermocline temperature gradient, and deep layer stratification. Analyzing nearly 15,000 Yellow Sea historical (1950–1988) temperature profiles (conductivity-temperature-depth station, 4825; expendable bathythermograph, 3213; bathythermograph, 6965) from the Naval Oceanographic Office's Master Oceanographic Observation Data Set by this parametric model, the Yellow Sea thermal field reveals dual structure: one layer (vertically uniform) during winter and multilayer (mixed layer, thermocline, sublayer) during summer. Strong seasonal variations were also found in mixed-layer depth, thermocline depth, and thermocline strength.

1. Introduction

The Yellow Sea is a semi-enclosed basin covering roughly 295,000 km^2 and is one of the most developed continental shelf areas in the world seas [*Yanagi and Takahashi*, 1993]. While the Yellow Sea covers a relatively large area, it is quite shallow, reaching a maximum depth of about 140 m (Figure 1). The water depth over most of the area is less than 50 m. The deepest water is confined to a north-south oriented trench which runs from the northern boundary south to the 100-m isobath, where it fans out onto the continental break. The gradients in slope across the bottom are very small. Such a broad and shallow continental shelf leads to the fact that the water is readily affected by seasonally varying atmospheric conditions such as heating, cooling, and wind stress. Therefore the seasonal variation of the water masses is remarkably large. Another feature of the depth distribution is the east/west asymmetry. Extensive shoals (<20 m) are located in the western Yellow Sea along the Chinese coast and are not generally found in the South Korea coastal regions. Also, the 50-m isobath is located more than 100 km from the Chinese coast but only about 50 km from the South Korea coast. This asymmetry in bottom depth is important for the shoaling mixed-layer depth. Furthermore, the hydrographic character of water masses in the Yellow Sea also depends on the degree of mixing of fresh water originating from the China continent river runoff with the intrusion of East China Sea and Kuroshio waters.

Before we sketch vertical structures of the Yellow Sea shelf water masses from the profiles, we should ask ourselves how can the thermal fields be described in terms of a set of characteristic parameters? In this study we developed a thermal parametric model to analyze 15,000 historical temperature profiles from the Naval Oceanographic Office (NAVOCEANO)'s Master Oceanographic Observation Data Set (MOODS) from the years 1950 to 1988 and to transform each temperature profile into a set of characteristic parameters such as sea surface temperature (SST), mixed-layer depth (MLD), thermocline depth, temperature difference across the thermocline, and the deep layer stratification.

Paper number 97JC00444.

2. Master Oceanographic Observation Data Set (MOODS)

The MOODS is a compilation of observed ocean data worldwide consisting of (1) temperature-only profiles, (2) both temperature and salinity profiles, (3) sound-speed profiles, and (4) surface temperatures from drifting buoys. These measurements are, in general, irregular in time and space. In this study we analyze temperature profiles measured from a variety of instruments. Due to the shear size (more than six million profiles) and enormous influx of data to NAVOCEANO from various sources, quality control is a difficult task. Our study domain includes the area 32°–41°N and 118°–127°E; the data set within this region consisted of nearly 15,000 profiles after rejecting certain data during quality control. These primary editing procedures included removal of profiles with obviously erroneous location, profiles with large spikes, and profiles displaying features that do not match the characteristics of surrounding profiles. In shallow water this procedure can be partially automated but also involves subjective interpretation because of the undersampling of MOODS compared to the spatial and temporal variability of the oceanography.

3. Seasonal Variation of the Atmospheric Forcing

The Asian monsoon strongly affects the Yellow Sea thermal structure. During the winter monsoon season a very cold

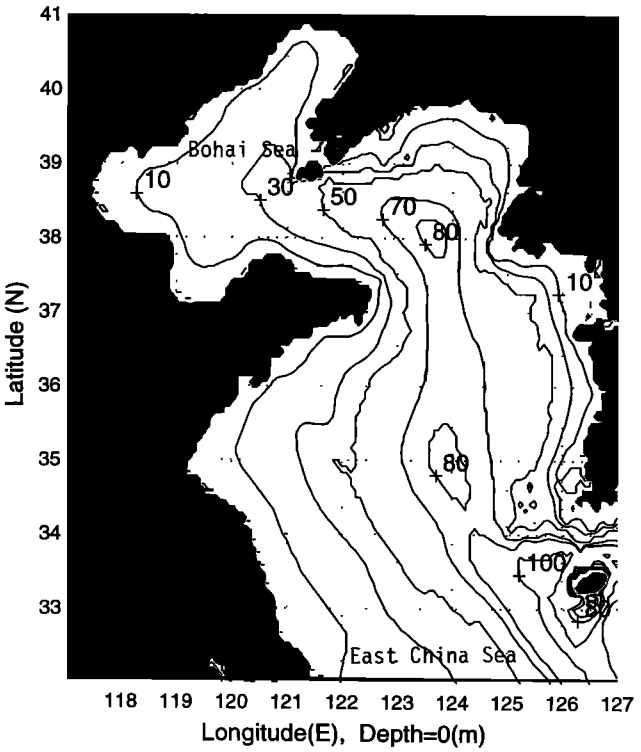

Figure 1. The Yellow Sea bathymetry. The data were obtained from the Naval Oceanographic Office DBDB5 world bathymetry database. Numbers show the depth (meters).

northwest wind blows over the Yellow Sea as a result of the Siberian high-pressure system. The jet stream is positioned to the south of the Yellow Sea and the polar front to the north of Philippines. The mean surface wind speed over the Yellow Sea in January is nearly 6 m/s (Figure 2a). The sea surface temperature is 6°C at the northern extent and 10°C at the southeastern extent. The January surface air temperature (SAT) varies from 0° to 8°C in the Yellow Sea, roughly 2°–6°C cooler than SST. The Yellow Sea surface loses heat to the atmosphere. The upward buoyancy flux at the air-ocean interface (thermal forcing), together with the strong wind stress (mechanical forcing), generates turbulence and mixes the surface water with the deeper water. The mixed layer is at its deepest (usually fills the whole water column) during winter owing to both convection and wind mixing by the strong northeast monsoon winds. The change of season begins in March when the surface air temperature is 5°C warmer than in February. Rapid weakening of the Siberian high progresses into April.

In late April the polar front has moved northward toward Korea with warm, moist air following behind. Numerous frontally generated events occur, making late April and May highly variable in terms of winds and cloud amount. By May the daily high surface air temperatures rise to 15°–16°C. During this period, storms originating in Mongolia may cause strong, warm westerlies carrying yellow desert sand (termed the "Yellow Wind"). By late May and early June the summer surface atmospheric low-pressure system begins to form over Asia. Initially, this low-pressure system is centered north of the Yellow Sea, producing westerly winds. In late June this low begins to migrate to the west, setting up the southwest monsoon that dominates the summer months. The winds remain variable through June until strengthening of the Manchurian low-pressure system occurs. The jet stream is just south of Korea, and the polar front is just south of Kyushu and Shikoku. Despite the very active weather systems the mean surface wind speed over the central Yellow Sea in summer is between 3 and 4 m/s, which is weaker than in winter (Figure 2b). June also marks, historically, a jump in precipitation associated with warm, moist air south of the polar front [*Watts*, 1969]. Occasionally, the Okhotsk high blocks the northerly progression of the polar front. By July, however, high pressure (the Bonin high) to the south and low pressure over Manchuria produce southerly winds carrying warm, moist air over the Yellow Sea. The summer monthly mean SAT is quite uniform, around 24°–26°C, and is usually 1.5°–2°C warmer than the mean SST [*Van Loon*, 1984]. The warmer air causes a downward heat flux at the air-ocean interface. This heat flux plus the strong downward net radiation stabilizes the upper layer of the water and

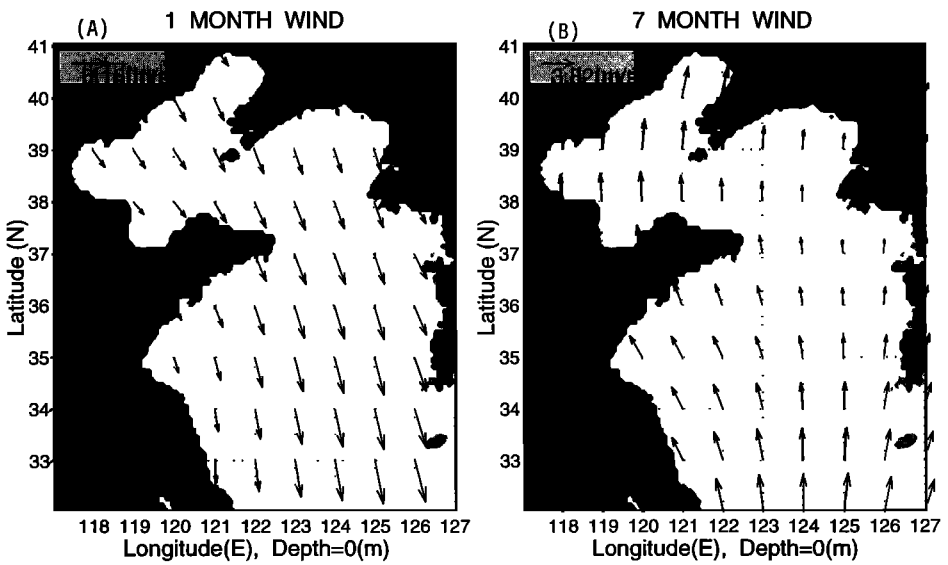

Figure 2. Mean atmospheric surface circulations in the vicinity of the Yellow Sea for (a) January and (b) July (computed from the European Centre for Medium-Range Weather Forecasts (ECMWF) data).

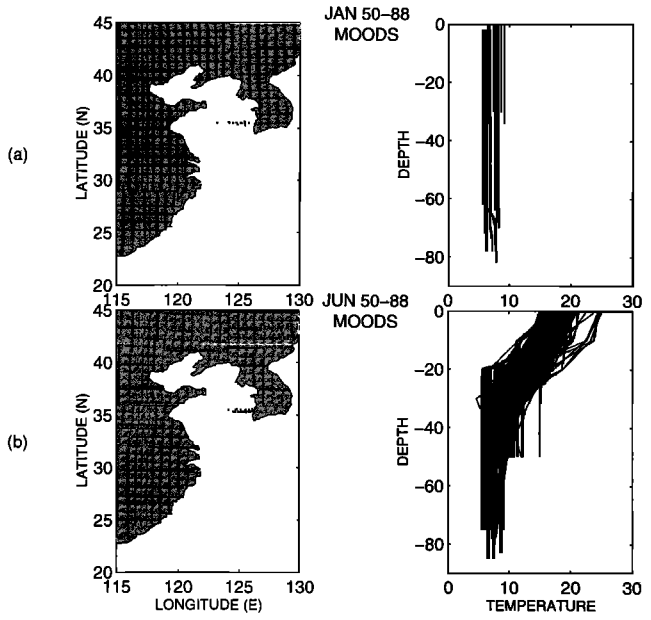

Figure 3. Eastern Yellow Sea (around 36°N) temperature profiles during 1950–1988: (a) January and (b) June. Solid squares show the observation stations.

causes the surface mixed layer to shoal, creating a multilayer structure. Below the thermocline, there is a cold water mass, commonly referred to as Yellow Sea Bottom Cold Water (YSBCW), that remains unchanged and nearly motionless throughout the summer [*Li and Yuan*, 1992]. October is the beginning of the transition back to winter conditions. The southerly winds weaken, letting the sea surface slope reestablish the winter pattern. The SST steadily decreases from October to January.

4. Seasonal Variation of Temperature Profiles

The Yellow Sea shelf water masses experience a strong seasonal variation (Figure 3). Taking the eastern part of the Yellow Sea around 36°N as an example, the January historical (1950–1988) temperature profiles (Figure 3a) show a single-layer structure (i.e., vertically uniform temperature from surface to bottom). The different lengths of these profiles in the vertical are caused by the different water depths where the observations were taken (see Figure 1). This single-layer structure means a very deep mixed layer extending from the surface to bottom. On the other hand, the June historical (1950–1988) temperature profiles (Figure 3b) indicate multilayer structure (i.e., mixed layer, thermocline, and deep layer). There also exists a shallow surface mixed layer in the summer profiles. Such a strong seasonal variation in vertical thermal structure is caused by a strong surface cooling in winter and a strong surface warming in summer.

5. Thermal Parametric Model

During the summer monsoon season, most profiles in the Yellow Sea exhibit a mixed layer, a thermocline, and a deep layer (Figure 3b), which can be outlined by a "typical" profile. To make the model more general, we assume two deep layers below the thermocline (Figure 4). When the two deep layers have the same vertical gradients, they become one deep layer. If two transition layers are added, the entrainment zone between the mixed layer and thermocline and the transition zone between the thermocline and the deep layer, the Yellow Sea thermal structure during summer can be well resolved. We use a parametric model with six layers [*Chu*, 1995] to diagnose shallow-water multilayer structure from observed Yellow Sea temperature profiles. Each observed profile is modeled by a set

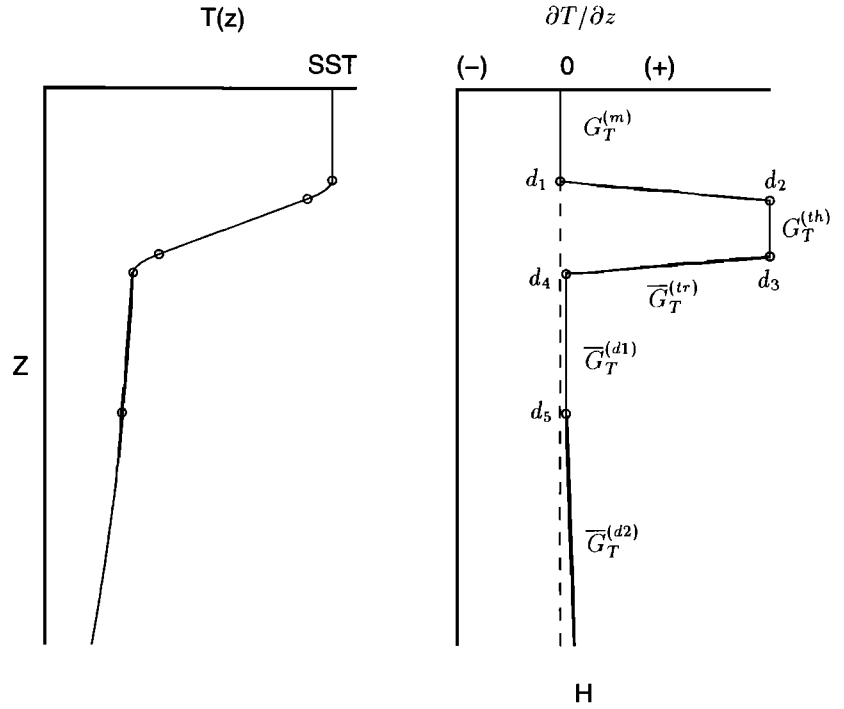

Figure 4. The temperature and gradient space representations of the features or profile characteristics modeled by the feature model.

of parameters, most of which have physical meaning, including SST, MLD, depth of the base of the thermocline, gradient in the thermocline and deep layers, and additional parameters describing curvature between the mixed layer and thermocline and curvature below the thermocline. Among them, SST is taken as the observed values. The model parameters for each observed profile are computed in gradient space; more specifically, the depths and gradients of the modeled features are fit to the vertical gradient of the observed profile. The parametric model depicts the multilayer structure. Determination of layer number is based on overall features of the profiles (Figure 3b). In this study the thermal parametric model consists of seven depths (i.e., six layers) and six gradients as shown in Figure 4. The first and last depths are assumed to be at the surface and bottom, respectively, and the gradients within the mixed layer and thermocline are constrained to be constant. The gradients for the four other layers are assumed to vary with depth linearly. The mean gradient is taken as the representative value for these layers. The model parameters are calculated in the gradient space, which will bring larger numerical errors due to the differentiation. We will use the optimization to filter out the noise.

5.1. Thermal Parametric Model

If we consider profiles in the gradient space, i.e., $G_T = \partial T(z)/\partial z$, each profile can be represented by the surface value (SST) plus the gradients, e.g.,

$$[\mathrm{SST},\ G_T(0, z_1),\ G_T(z_1, z_2),\ \cdots,\ G_T(z_{n-1}, z_n)]$$

for the temperature profiles. Here, $n + 1$, is the number of data points, and $z_i (i = 1, 2, \cdots, n)$ are the depths of the subsurface data points. For example, 100 temperature/depth points would produce 99 gradient values. If the surface value is included, we have the same amount of data in the gradient space as in the original data set.

On the basis of the continuity of T and $\partial T/\partial z$ at interfaces of any two layers, a parametric model can be constructed as

$$\hat{T}^{(m)}(z) = G_T^{(m)} z + \mathrm{SST} \qquad z \in [-d_1, 0] \tag{1a}$$

$$\hat{T}^{(en)}(z) = \frac{(z + d_1)}{2(d_2 - d_1)} \cdot [(G_T^{(th)} + G_T^{(m)})(d_2 - d_1) - (G_T^{(th)} - G_T^{(m)}) \cdot (z + d_2)] + \hat{T}^{(m)}(-d_1) \qquad z \in [-d_2, -d_1] \tag{1b}$$

$$\hat{T}^{(th)}(z) = G_T^{(th)}(z + d_2) + \hat{T}^{(en)}(-d_2) \quad z \in [-d_3, -d_2] \tag{1c}$$

$$\hat{T}^{(tr)}(z) = \frac{(z + d_3)}{(d_4 - d_3)} [(G_T^{(th)} - \bar{G}_T^{(tr)})z + d_4 G_T^{(th)} - d_3 \bar{G}_T^{(tr)}] + \hat{T}^{(th)}(-d_3) \qquad z \in [-d_4, -d_3] \tag{1d}$$

$$\hat{T}^{(d1)}(z) = \hat{T}^{(tr)}(-d_4) + (z + d_4)\bar{G}_T^{(d1)} + \frac{(z + d_4)(z + d_5)}{d_5 - d_4} \cdot [G_T^{(tr)}(-d_4) - \bar{G}_T^{(d1)}] \qquad z \in [-d_5, -d_4] \tag{1e}$$

$$\hat{T}^{(d2)}(z) = \hat{T}^{(d1)}(-d_5) + (z + d_5)\bar{G}_T^{(d2)} + \frac{(z + d_5)(z + H)}{H - d_5} \cdot [G_T^{(d1)}(-d_5) - \bar{G}_T^{(d2)}] \qquad z \in [-H, -d_5] \tag{1f}$$

where $\hat{T}^{(m)}$, $\hat{T}^{(en)}$, $\hat{T}^{(th)}$, $\hat{T}^{(tr)}$, $\hat{T}^{(d1)}$, and $\hat{T}^{(d2)}$ are modeled temperatures in the mixed layer, the entrainment zone, the thermocline, the transition zone, and the first and the second deep layers, respectively. H is the water depth, d_1 is the mixed-layer depth, d_2 is the depth of the thermocline top, d_3 is the depth of the thermocline bottom, d_4 is the depth of the top of the first deep layer, and d_5 is the bottom of the first deep layer (Figure 4). Here we assume constant vertical temperature gradients in the ocean mixed layer (very small, $G_T^{(m)} \approx 0$) and in the thermocline (very large $G_T^{(th)}$) and linearly varying with z in the entrainment zone, the transition zone, and the two deep layers add with average values $\bar{G}_T^{(en)}$, $\bar{G}_T^{(tr)}$, $\bar{G}_T^{(d1)}$, and $\bar{G}_T^{(d2)}$. Here the mean gradient in the entrainment zone is the average of the mixed-layer and thermocline gradients, i.e., $\bar{G}_T^{(en)} = (G_T^{(m)} + G_T^{(th)})/2$. By forcing this parametric model (1a)–(1f) to each observed profile, we should have a first guess of the five depths (d_1, d_2, d_3, d_4, d_5) and a high resolution of temperature/depth points in the vertical in order to obtain the five temperature gradients ($G_T^{(m)}$, $G_T^{(th)}$, $\bar{G}_T^{(tr)}$, $\bar{G}_T^{(d1)}$, $\bar{G}_T^{(d2)}$). Such a treatment provides the most important features from the observational data.

5.2. High-Resolution Profiles (HP) Interpolated From Observations

Each MOODS profile is linearly interpolated to $\Delta z = 0.5$ m, $T_j = T(z_j)$, where $z_j = z_{j-1} - 0.5$ m ($z_0 = 0$). The NAVOCEANO's Digital Bathymetric Data Base 5 (DBDB5) data set is used to obtain water depth H. If the five depths (d_1, d_2, d_3, d_4, d_5) are known, we can divide the data set HP = (z_j, T_j) into six parts (mixed layer, entrainment zone, thermocline, transition zone, first deep layer, and second deep layer). For each layer we fit (T_j, z_j) to the parametric model (1a)–(1f) and obtain a set of temperature gradients ($G_T^{(m)}$, $G_T^{(th)}$, $\bar{G}_T^{(tr)}$, $\bar{G}_T^{(d1)}$, $\bar{G}_T^{(d2)}$).

5.3. Modeled Profile (MP) Obtained by the Iteration Method

A modeled profile (MP) with 0.5-m resolution can be established by using the parametric model (1a)–(1f) if the five depths (d_1, d_2, d_3, d_4, d_5) are given. In reality these depths are not known prior to processing the data and vary from one profile to the other. We use the iteration method to obtain the optimal MP.

First, we start with a set of first-guess values of the depths and the five gradients (two constants and three mean values),

$$D^{(0)} = (d_1^{(0)}, d_2^{(0)}, d_3^{(0)}, d_4^{(0)}, d_5^{(0)}),$$
$$G_T^{(0)} = (G_T^{(m_0)}, G_T^{(th_0)}, \bar{G}_T^{(tr_0)}, \bar{G}_T^{(d1_0)}, \bar{G}_T^{(d2_0)}). \tag{2}$$

In this study we choose

$$D^{(0)} = (20\ \mathrm{m}, 24\ \mathrm{m}, 32\ \mathrm{m}, 38\ \mathrm{m}, H)$$
$$G_T^{(0)} = (0,\ 0.5°\mathrm{C/m},\ 0.005°\mathrm{C/m},\ 0,\ 0).$$

For each HP profile we fit the data (z_j, T_j) to the parametric model (1a)–(1f) since we know the depths and the gradients and obtain a zeroth-order modeled profile, called $\mathrm{MP}^{(0)} = (z_j, \hat{T}_j^{(0)})$. The RMS error for mismatch of HP and $\mathrm{MP}^{(0)}$ is computed by

$$\mathrm{RMS}^{(k)} = \sqrt{\frac{1}{n}\sum_{j=1}^{n} (\hat{T}_j^{(k)} - T_j)^2} \tag{3}$$

where $k = 0$. We expect $\mathrm{RMS}^{(0)}$ to be large.

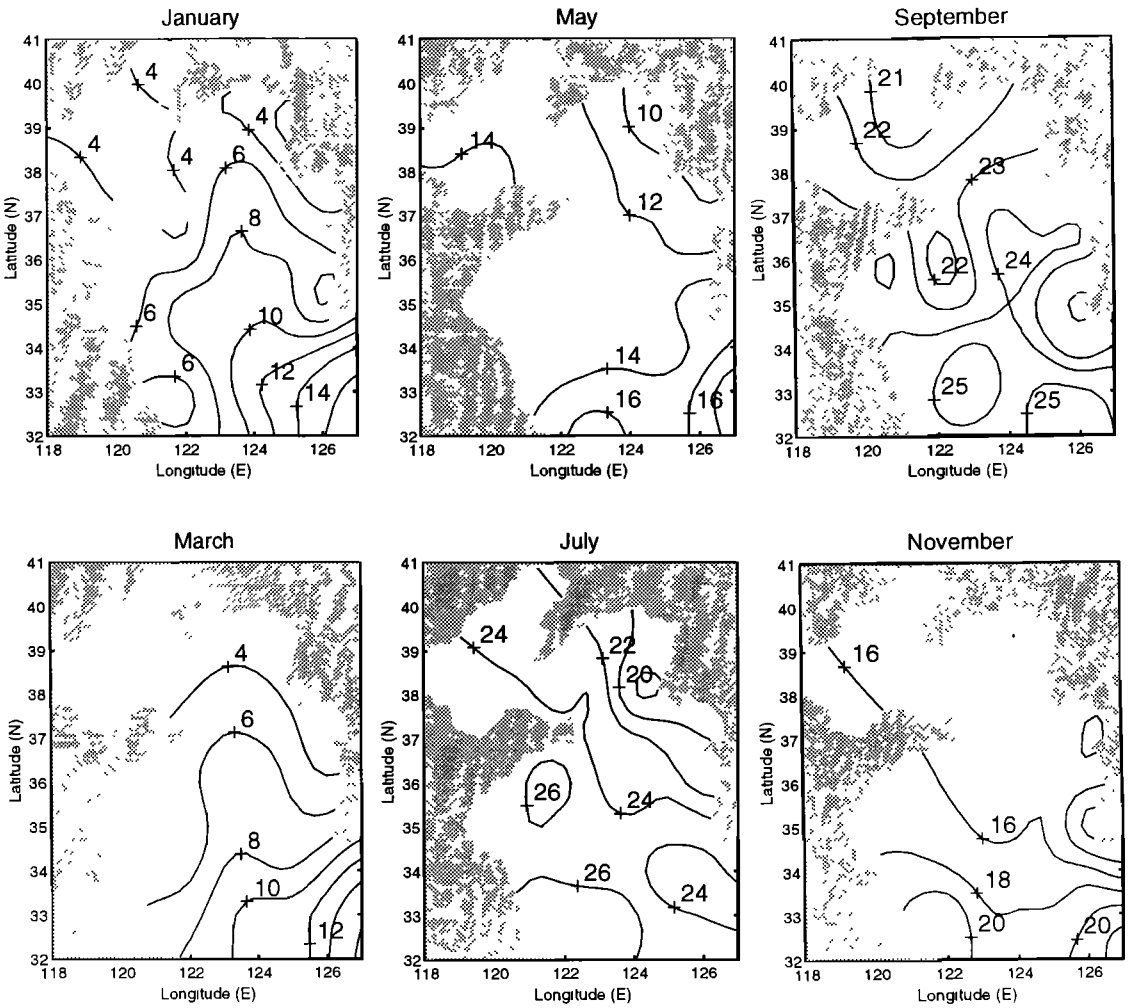

Figure 5. Bimonthly variation of SST. Data were obtained from the MOODS for the years 1950–1988.

Second, we use the iteration method to obtain optimal MP for each HP profile. Each depth can only be adjusted one vertical grid (Δz or $-\Delta z$) for one iteration. From the kth-order (k starting from 0, the first guess) set of depths, $D^{(k)}$, we have 242($= 3^5 - 1$) different combinations of the depth adjustment,

$$D_m^{(k+1)} = D^{(k)} + \delta D_m^{(k)}, \tag{4}$$

where

$$\delta D_1^{(k)} = (\Delta z, 0, 0, 0, 0),$$
$$\delta D_2^{(k)} = (-\Delta z, 0, 0, 0, 0),$$
$$\vdots$$
$$\delta D_{242}^{(k)} = (0, 0, 0, 0, -\Delta z).$$

We use (1a)–(1f) to obtain 242 modeled profiles, among which we pick a profile with minimum RMS error as the $(k + 1)$th-order set of depths, $D^{(k+1)}$. We repeat this procedure until the minimum RMS error is achieved. We have two check points to terminate the iteration: the maximum number of iterations $k_{\max}$ and the RMS error criterion R_c. At each iteration ($k < k_{\max}$), $\mathrm{RMS}^{(k)}$ is compared to a user-specified criterion R_c. If $\mathrm{RMS}^{(k)} < R_c$, we terminate the iteration and obtain an optimal set of depths. If $\mathrm{RMS}^{(k)} > R_c$, we continue the iteration until $k = k_{\max}$. If the RMS error at the $k_{\max}$ iteration is still greater than R_c, we should reject the parametric model (1a)–(1f); that is, the HP profile cannot be fitted by the parametric model. The rejected profiles are discarded. In this study we chose $k_{\max} = 400$, $R_c = 0.4$°C. This RMS criterion (0.4°C) was chosen due to the accuracy of the temperature/depth (±0.2°C, ±2 m) measured by the bathythermograph (BT). If the data are obtained by more accurate instruments (e.g., thermometer), this criterion can be greatly reduced. The number of rejected profiles is 1232. The six temperature gradients were updated at each iteration. A set of the six optimal gradients is obtained when the RMS error of the temperature profile is less than the criterion.

6. Yellow Sea Shelf Thermal Features

The parametric model (1a)–(1f) transforms any profile (if not rejected) into a set of five depths (d_1, d_2, d_3, d_4, d_5) and six gradients ($G_T^{(m)}$, $G_T^{(th)}$, $\bar{G}_T^{(en)}$, $\bar{G}_T^{(tr)}$, $\bar{G}_T^{(d1)}$, $\bar{G}_T^{(d2)}$). These parameters represent the most important physical features and are insensitive to the first-guess values. The first-guess values only affect the number of iterations. A good selection of first-guess values reduces the number of iterations. Since winter (December–April) profiles reveal a single-layer structure [*Fralick*, 1994], the set of characteristic parameters

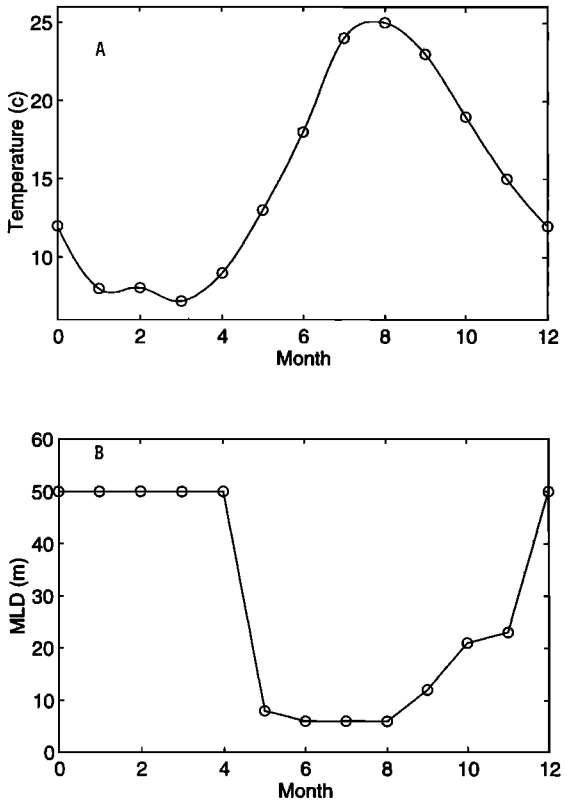

Figure 6. Monthly variation of the central Yellow Sea (123°–124°E, 36°–37°N) thermal features: (a) SST (degrees Celsius) and (b) MLD (meters).

reduces to (SST, H). Therefore the thermal parametric model was used to process only summer monsoon season (May–November) profiles. Due to the data sparsity, the summer profiles with the same month and different years were grouped together to obtain the characteristic parameters of the monthly variations.

6.1. Seasonal Variation of Sea Surface Temperature

Bimonthly evolution of SST (Figure 5), constructed from the MOODS data (1950–1988), shows some interesting features which are summarized as follows.

1. During the winter monsoon season, SST has a weak temporal variation. In the central Yellow Sea, SST decreases slowly cooling rate ~−4°C/month) from November through January, stays almost the same (6°–8°C) from January through March, and increases slowly (warming rate ~−3°C/month) from March through May. The heat loss (or gain) at the ocean surface cools (or warms) the whole column of the water, causing a slow change of SST.

2. The winter SST (January, March) shows a tongue-like distribution which extends from southeast to northwest, which coincides with observations collected during a single year (1986) in the Yellow Sea [*Chen et al.*, 1994]. Such a tongue-like structure implies the existence of the Yellow Sea Warm Current (YSWC) in winter [*Hsueh*, 1988].

3. During the summer monsoon season, on the other hand, SST has a strong temporal variation. In the central Yellow Sea, SST increases rapidly from May through July (warming rate ~7°C/month) and stays warm (above 20°C) through September. SST noticeably cools from September through December (~−4°C/month). The rapid change is due to a shallower mixed layer during the summer monsoon season. The heat gain (or loss) at the ocean surface warms (or cools) only the mixed layer, causing a rapid change of SST.

4. The seasonal variation of sea surface temperature has its the largest value (~20°C) in the northern Yellow Sea (north of 37°N) and decreases southward.

The SST over the Yellow Sea has a strong annual cycle. In the central Yellow Sea (123°–124°E, 36°–37°N) the maximum SST (25.2°C) appears in late July and early August, and the minimum SST (7°C) occurs in March (Figure 6a).

6.2. Mixed-Layer Depth

By late winter the water throughout the Yellow Sea is very isothermal. During onset of the summer monsoon an increase in the solar insolation and weakening winds begin the stratification process on the Yellow Sea Shelf. This is supported by a strong annual cycle of MLD in the central Yellow Sea (123°–124°E, 36°–37°N). During the winter monsoon season (December–March), MLD has the same value (~50 m) as the water depth (single-layer structure). During the onset of the summer monsoon, MLD reduces drastically from 50 to 8 m (multilayer structure due to stratification) and then keeps small values (less than 8 m) throughout the whole summer season (Figure 6b).

The Yellow Sea bimonthly progression of the MLD plots (Figure 7) reveals some interesting features:

1. There are two stages for the time evolution of mixed-layer depth: a quasi-steady (and shallow) stage from May through July and an evident deepening stage from July through November.

2. The contours of the mixed-layer depth almost follow the bathymetry (Figure 1). The central Yellow Sea has a relatively deep mixed layer during the whole summer monsoon season, whose depth is from 5 to 10 m for the quasi-steady stage (under very weak surface forcing) and deepens to 20–25 m during an evident deepening stage caused by reduced insolation and increased wind.

3. The mixed-layer depth is very shallow (~5 m) in the north Yellow Sea (north of 37°N) during the quasi-steady stage and increases to 15–20 m during the evident deepening stage. The shallow mixed layer in the first stage is very sensitive to the net surface heat flux.

4. Large mixed-layer depth occurs during the transition month of November, when solar insolation has decreased markedly and winds have picked up.

5. The mixed-layer depth is also affected by the large discharge from surrounding rivers (Yangtze River, Huangho River, etc.). As reported by *Yang et al.* [1983], the discharge from the Yangtze River is maximum in July (16% of annual discharge) and minimum in January (3% of annual discharge). Near the Chinese coast the mixed-layer depth is minimum in July (less than 2 m).

6. The mixed-layer depth is strongly influenced by tidal mixing in shallow regions such as along the Chinese coast in water less than 20 m deep. The amplitudes of M_2 and S_2 tides there are larger south of 34°N than north of 34°N [*Yanagi and Inoue*, 1994], which implies stronger tidal vertical mixing (in turn thicker mixed layer) south of 34°N. This can be clearly seen in September and November MLD plots (Figure 7).

6.3. Prominence of the Seasonal Thermocline

July is a month of strong surface heating as witnessed by the sharp increase in SST shown in Figure 5. As a result the

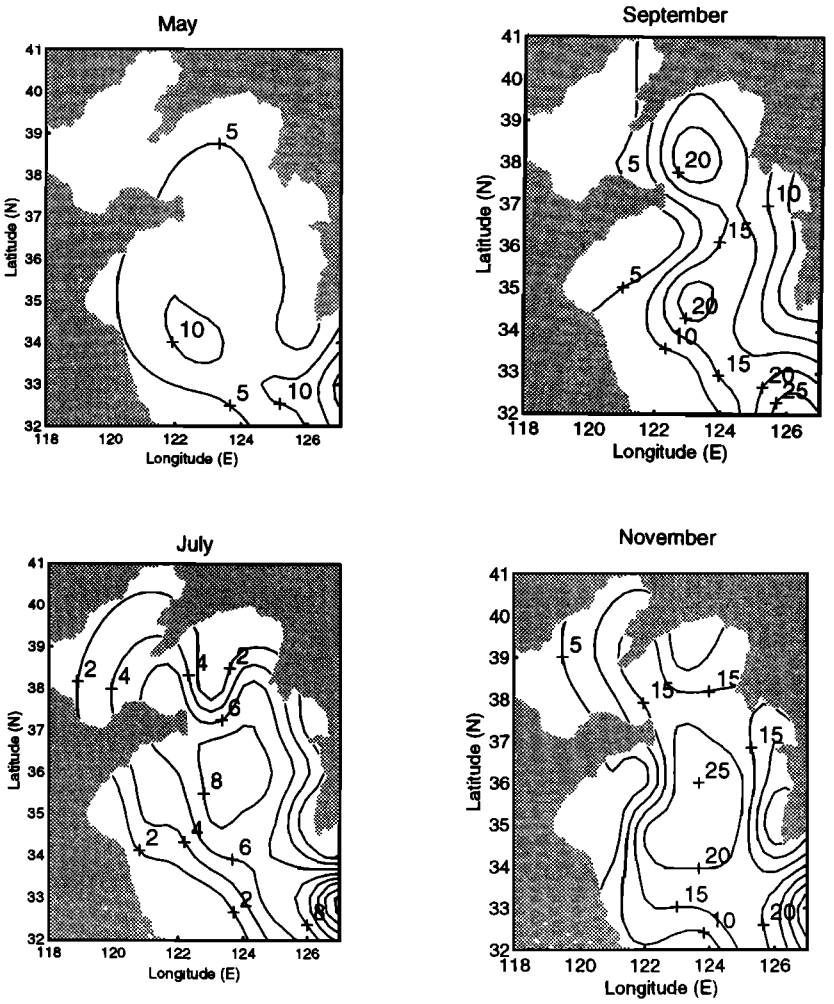

Figure 7. Bimonthly evolution of MLD (meters) in the Yellow Sea. Data were gridded and horizontally interpolated from the MOODS for the years 1950–1988.

prominence of the thermocline is expected. With the presence of YSBCW in the central region a positive temperature gradient across the thermocline should be apparent and appears in the central part of the Yellow Sea shelf. The presence of this centrally manifested gradient is more obvious in August and shows a stronger gradient as summer progresses. September shows a ridge in the temperature gradient distribution oriented north-south in the central region which suggests the deeper, colder water serves to maintain the temperature difference even into the later summer. As solar insolation decreases in October and wind speeds begin to increase, entrainment begins at the mixed-layer base to break down the thermocline. This is borne out by the October map where the north-south oriented ridge in temperature gradient is still present but the magnitude of the gradient has decreased significantly.

The temperature difference across the thermocline, $\Delta T^{(th)}$, is computed from the output of the parametric model, d_2, d_3, and $G^{(th)}$,

$$\Delta T^{(th)} = G^{(th)}(d_3 - d_2) \tag{5}$$

The bimonthly evolution of $\Delta T^{(th)}$ field (Figure 8) indicates some important features.

1. The contour of $\Delta T^{(th)}$ almost follows the bottom topography (Figure 1). No matter which month in the year, the maximum $\Delta T^{(th)}$ always appears in the central Yellow Sea. This phenomenon can be explained by the tidal vertical mixing [*Yanagi and Inoue*, 1994; *Takahashi and Yanae*, 1995]. The circulations in the Yellow Sea during summer are mainly induced by the sea surface heating and are affected by the vertical mixing of the tidal current and the bottom topography. The homogeneous water which is formed by the sea surface cooling in winter begins to stratify due to the sea surface heating in spring. However, due to the horizontal difference of the tidal vertical mixing effect (stronger tidal mixing in shallow shelves), the intensity of the stratification in the central Yellow Sea becomes stronger than the surrounding part. Besides, surface heating during the summer monsoon season also shoals the mixed layer and makes the mixed-layer temperature (i.e., SST) relatively uniform horizontally. Since the minimum temperature in the deeper layer appears in the central Yellow Sea (i.e., YSBCW), a strong thermocline should be located there.

2. The thermocline strengthens during the first half of the summer monsoon season (May–July). The maximum $\Delta T^{(th)}$ increases from 5°C in May to 14°C in July. During the second half of the summer monsoon season (July–September) the thermocline weakens except in the central Yellow Sea where the thermocline strength remains high value (maximum $\Delta T^{(th)} \sim 14$°C). The strength of the thermocline further

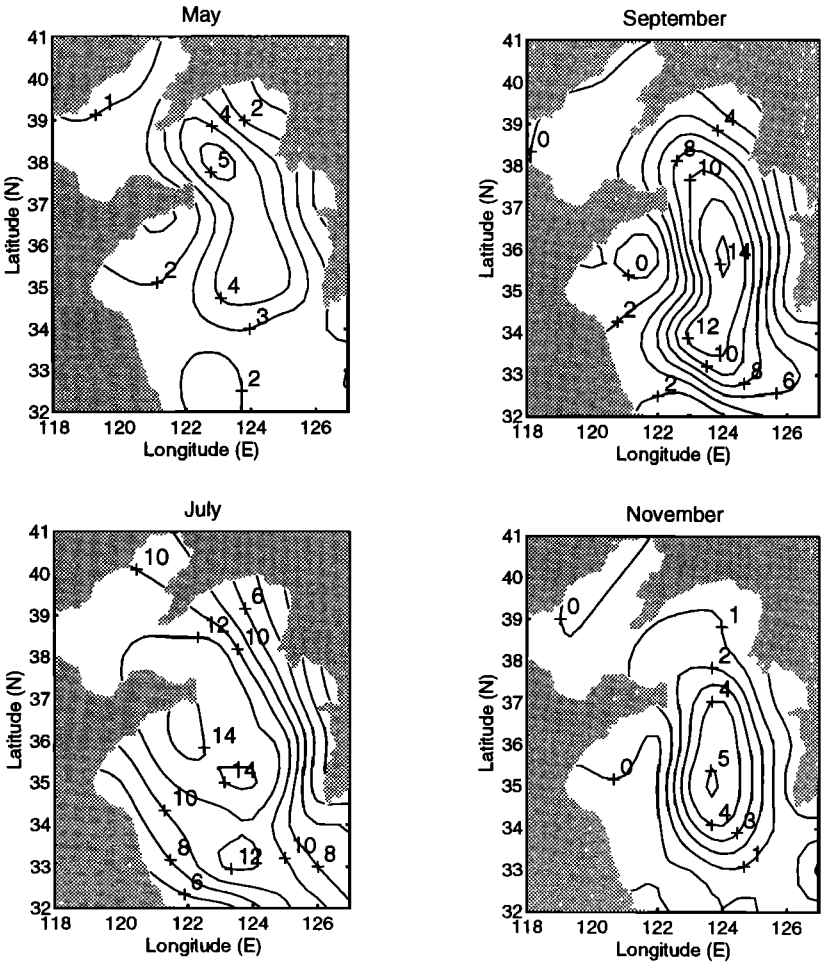

Figure 8. Thermocline temperature difference (degrees Celsius) in the Yellow Sea from May to November. Data were obtained from the MOODS for the years 1950–1988.

reduces from September through November (maximum $\Delta T^{(th)} \sim 5°C$). During the winter monsoon season (December–April) the Yellow Sea waters are well mixed vertically, and there is no thermocline during that period.

7. Conclusion

1. The thermal parametric model depicted in this paper demonstrates a good capability to compress a large data set into a small enough volume of data such that the investigators may readily assimilate and interpret it. The model clearly shows large thermal variabilities and the dual structure of the Yellow Sea shelf: a one-layer structure during the winter monsoon season (December–April) and a multilayer structure during the summer monsoon season (May–November).

2. The Yellow Sea surface mixed layer has more thermal inertia during winter monsoon season than summer monsoon season. SST stays almost the same from January through March (winter monsoon) and, increases dramatically from May through July (summer monsoon season). The maximum warming rate (7°C/month) in summer is nearly 2 times higher than the cooling rate ($<-4°C$/month) in winter. The seasonal variation of SST has its largest value (20°C) in the northern Yellow Sea and decreases southward.

3. During the winter monsoon season the surface mixed layer extends from the surface to the bottom. After the onset of the summer monsoon in May the ocean mixed layer shoals and experiences two stages of evolution. A quasi-steady and shallow stage (MLD ~ 10 m at the central Yellow Sea) appears from May through August, and an evident deepening stage (MLD ~ 20–25 m at the central Yellow Sea) occurs from August through November. During the first stage the mixed layer has the least thermal inertia and is sensitive to surface thermal forcing.

4. A strong thermocline occurs during the summer monsoon season, with the largest $\Delta T^{(th)}$ occurring in September. The thermocline strengthens continuously after the onset of the summer monsoon season. The maximum $\Delta T^{(th)}$ for the Yellow Sea increases from 5°C in May to 14°C in July and is maintained (maximum $\Delta T^{(th)} \sim 14°C$) through September. The strength of the thermocline decreases from September through November (maximum $\Delta T^{(th)} \sim 5°C$). During the winter monsoon season the Yellow Sea waters are vertically well mixed, with little or no stratification.

5. The thermal structure is affected by the air-sea surface heat flux, the wind, the tidal vertical mixing, and the large discharge from the mainland of China (Yangtze River, Huangho River, etc.). The Yellow Sea lies within the Asian monsoon circulation and experiences hot, humid summers and long, cold, dry winters. In winter the Yellow Sea is dominated by the cold northerly wind associated with the Siberian high.

The SST is 6°C at the northern extent and 10°C at the southeast extent. The January to surface air temperature (SAT) varies from 0° to 8°C in the Yellow Sea [*Chu et al.*, 1997], roughly 2°–6°C cooler than SST. The Yellow Sea surface loses tremendous heat to the atmosphere. The upward buoyancy flux at the air-ocean interface (thermal forcing), together with the strong wind stress (mechanical forcing), generates turbulence and mixes the surface water with the deeper water. The mixed layer is at its deepest (it usually fills the whole water column) during winter owing to both convection and wind mixing by the strong northeast monsoon winds. In summer the Yellow Sea is dominated by the warm and moist southwesterly wind associated with the atmospheric low-pressure system over Asia (the Manchurian low) and high-pressure system in the southeast (the Bonin high). The summer SAT is quite uniform and around 24°–26°C [see *Chu et al.*, 1997]. It is usually 1.5°–2°C warmer than SST [*Van Loon*, 1984]. The warmer air brings downward heat flux at the air-ocean interface. This heat flux plus the strong downward net radiation stabilizes the upper layer of the water and causes the surface mixed layer to shoal. Furthermore, near the Chinese coast the MLD has a minimum in July (less than 2 m). This is mainly due to the maximum freshwater influx at the major river mouths in July. The mixed-layer depth at the southwest corner of the Yellow Sea (near the Yangtze River mouth) increases from 2 m in July to the whole water column in November.

6. This parametric model can also be used to process output from any dynamical model and to obtain meaningful products, i.e., MLD, thermocline depth, thermocline strength, and deep layer stratification.

Acknowledgments. The authors are grateful to Laura Ehret, Michael Cook, and C. W. Fan at the Naval Postgraduate School for their programming assistance. This work was funded by the Naval Oceanographic Office, the Office of Naval Research NOMP and PO Programs, and the Naval Postgraduate School.

References

Chen, C. S., R. C. Beardsley, R. Limeburner, and K. Kim, Comparison of winter and summer hydrographic observations in the Yellow and East China Seas and adjacent Kuroshio during 1986, *Cont. Shelf Res.*, *14*, 909–929, 1994.

Chu, P. C., A feature model for Arctic upper ocean thermal structure, in *Proceedings, the Fourth Conference on Polar Meteorology and Oceanography*, pp. 224–227, Am. Meteorol. Soc., Boston, Mass., 1995.

Chu, P. C., S. K. Wells, S. D. Haeger, C. Szczechowski, and M. J. Carron, Temporal and spatial scales of the Yellow Sea thermal variability, *J. Geophys. Res.*, *102*, 5655–5667, 1997.

Fralick, C. R., Jr., Yellow Sea thermal structure, M.S. thesis, U.S. Nav. Postgrad. School, Monterey, Calif., 1994.

Hsueh, Y., Recent current observation in the eastern Yellow Sea, *J. Geophys. Res.*, *93*, 6875–6884, 1988.

Li, H., and Y. Yuan, On the formation and maintenance mechanisms of the cold water mass of the Yellow Sea, *Chin. J. Oceanol. Limnol.*, *10*(2), 97–106, 1992.

Takahashi, S., and T. Yanagi, A numerical study on the formation of circulations in the Yellow Sea during summer, *La Mer*, *33*, 135–147, 1995.

Van Loon, H., Climates of the oceans, *World Surv. Climatol.*, *15*, 453–458, 1984.

Watts, I. E. M., Climates of China and Korea, *World Surv. Climatol.*, *8*, 1–117, 1969.

Yanagi, T., and K. Inoue, Tide and tidal current in the Yellow/East China Seas, *La Mer*, *32*, 153–165, 1994.

Yanagi, T., and S. Takahashi, Seasonal variation of circulations in the East China Sea and the Yellow Sea, *J. Oceanogr.*, *49*, 503–520, 1993.

Yang, Z. S., J. D. Milliman, and M. G. Fitzgerald, Transfer of water and sediment from the Yangtze River to the East China Sea, June, 1980, *Can. J. Fish. Aquat. Sci.*, *40*, 72–82, 1983.

M. J. Carron and S. D. Haeger, Naval Oceanographic Office, Stennis Space Center, MS 39529.

P. C. Chu and C. R. Fralick Jr., Naval Postgraduate School, Code OC/CU, Monterey, CA 93943. (e-mail: chu@nps.navy.mil)

(Received August 13, 1996; revised January 3, 1997; accepted January 23, 1997.)